Desalination and Water Treatment
www.deswater.com

doi: 10.5004/dwt.2021.27200

224 (2021) 122–135
June

O-MWCNT/PAN/PVDF ultrafiltration membranes with boosted properties for oil and water separation

Temitope F. Ajibade[a,b], Jiaoxing Xu[c], Huali Tian[a], Lunhui Guan[c], Kaisong Zhang[a,*]

[a]*Key Laboratory of Urban Pollutant Conversion, Institute of Urban Environment, Chinese Academy of Sciences, Xiamen 361021, China, emails: kszhang@iue.ac.cn (K. Zhang), temitope@iue.ac.cn (T.F. Ajibade), hltian@iue.ac.cn (H. Tian)*
[b]*Department of Civil and Environmental Engineering, Federal University of Technology Akure, PMB 704 Akure, Nigeria*
[c]*CAS Key Laboratory of Design and Assembly of Functional Nanostructures, Fujian Provincial Key Laboratory of Nanomaterials, Fujian Institute of Research on the Structure of Matter, Chinese Academy of Sciences, Fuzhou, Fujian 350108, China, emails: xujx_1220@fjirsm.ac.cn (J. Xu), guanlh@fjirsm.ac.cn (L. Guan)*

Received 25 November 2020; Accepted 3 March 2021

ABSTRACT

Removal of emulsified oil droplets less than 20 μm and maintaining operational stability remains a key concern in the field of oily wastewater treatment. In this work, a major breakthrough was achieved via modification of polyacrylonitrile/polyvinylidene fluoride (PAN/PVDF) blended ultrafiltration (UF) membrane with oxidized multiwall carbon nanotubes (O-MWCNT) to tailor the membrane chemical properties for boosted oil and water separation. Overall, a high separation performance of oily emulsion (99%) and simultaneous increase in flux up to 65% was achieved using the novel O-MWCNT/PAN/PVDF membrane. Moreover, the performance of the O-MWCNT/PAN/PVDF membrane was consistent after 28-cycles of oil separation and the antifouling properties were exceptionally enhanced by 96%. In addition, there was a significant decrease in fouling in terms of the cake, pore, and intrinsic resistance. Furthermore, evidence of even dispersal of nanofillers was confirmed by an increase of casting solution viscosity with increasing O-MWCNT. Consequently, this provides a remarkable mechanical/tensile strength of 5.94 MPa, and 16.05% elongation of the O-MWCNT/PAN/PVDF fingerlike structured UF membrane. The novel O-MWCNT/PAN/PVDF membrane demonstrated promising properties that balanced the membrane tradeoff between permeability and selectivity, as well as, improved mechanical strength and operational stability that can elongate the life span of the membrane in oily wastewater treatment.

Keywords: Oily wastewater; O-MWCNT; PAN/PVDF; Mechanical strength; Ultrafiltration

1. Introduction

Over the years, extensive awareness has been drawn to oily waste purification technology due to the adverse effect of oily wastewater pollution on the environment. The water bodies are mostly affected by the large volume of oily wastewater produced from petrochemical, oil and gas, food, and textile industries [1]. Apart from the toxicity accompanied by oily wastewater, they contain petroleum and polyaromatic hydrocarbon that impede growth in plants and animals [2]. Besides, the available limited freshwater resources, which are usually utilized as the primary sources of water consumption cannot optimally meet the daily demand, leading to the invention of new water separation and recycling technologies [3]. Conventional separation techniques such as coagulation, gravity separation, flocculation, flotation, and chemical methods have been employed for oily wastewater separation [4–6]. However, these techniques only address

* Corresponding author.

immiscible oily wastewater with oil droplet size more than 150 μm and in some cases oil size between 20 and 150 μm. Till now, challenges exist dealing with emulsified oily wastewater of droplet size less than 20 μm [7,8].

Among other separation techniques, the membrane separation method has been of great interest over the past few decades for the purification of oily wastewater of droplets less than 20 μm using the principle of wettability and sieving effect [9,10]. For example, Peng et al. [7] fabricated and modified a polyacrylonitrile (PAN) membrane for the separation of an emulsified oily wastewater, the result revealed separation efficiency for COD between 200 and 600 mg/L. Similarly, Zhang et al. [11] fabricated an alkaline-induced PAN membrane for the same purpose, and the result depicted that the oil residuals were less than 10 mg/L after filtration. Generally, to effectively separate emulsified oil using a membrane, the membrane should be hydrophilic and underwater oleophobic. These properties are essential because hydrophilicity permits the smooth flow of water while the oleophobic property prevents the flow of oil through the membrane [11,12]. However, the deposition of tiny oil droplet size on the surface and within the pores of the membrane has led to membrane oil fouling which remains a critical issue limiting the application of membrane in the industrial sector [13,14]. The top/active layer of a membrane enacts a major role in the performance of the membrane, as it can enhance the adsorption of particles on its surface. Consequently, fouling can be reduced by improving or refining the properties (surface charge, roughness, and hydrophilicity) of the top layer of the membrane. A known approach toward tackling the fouling behavior of a membrane involves implementing the theory of hydrophilicity, that is, creating a robust hydration layer that obstructs the adsorption of foulant on the surface of the membrane [15,16].

One common method for increasing the hydrophilicity of conventional polymer membrane is by polymer blending, which is also known as grafting. In this method, a hydrophilic membrane is grafted with a hydrophobic membrane at a specific weight ratio(s) to increase superficial hydrophilicity [17]. Moreover, this process is useful for improving polymer properties, fabricating new types of materials and has demonstrated superb quality for application in different fields. A key factor usually considered in polymer blending is the compatibility of the polymers which has a significant influence on the structure and the properties of the modified membrane. The compatibility of the polymers is often based on the thermodynamics stability (heat of mixing), which is influenced by the molecular parameters of the polymers [18]. The free energy of mixing (ΔG_m) from the interaction between these parameters could be obtained from the difference between the enthalpy and the entropy of mixing. For most polymers, the entropy of mixing is negligible, consequently, the enthalpy of mixing determines the compatibility of the polymers [19]. Another parameter that contributes to the enthalpy of mixing is the repulsive reaction between the monomer residues of the polymer, such that a weaker repulsive interaction tends to favor the miscibility of polymers [20]. Schneier's theory is mostly used to determine the compatibility of polymer blends at a particular weight ratio in which a resultant enthalpy value (ΔH_m) more than 0.01 cal/mol indicates that the polymers are incompatible while the ΔH_m, that is, less than 0.01 cal/mol indicates that the polymers are compatible [21]. Masheane et al. [22] applied this theory to investigate the compatibility of polyethersulfone (PES) and quaternized-PES blend anion exchange membrane, which revealed that the polymer blend with ΔH_m below 0.01 cal/mol displayed thermodynamic stability while ΔH_m above 0.01 cal/mol shows thermodynamic instability and immediate demixing [22]. Similarly, Li et al. [17] used this theory to determine the effect of sulfonated polysulfone on the compatibility with PES-based polymer blend, the result confirmed that the polymers were completely miscible at all weight ratio. Furthermore, many other researchers have worked on different polymer blend such as PAN/polyvinylidene fluoride (PVDF) [23,24], PVDF/sulfonate polycarbonate [25], PVDF-co-HFP/PAN [26], PVDF/polyethylene glycol (PEG) [27], in which the resulting membranes indicated improved polymeric membrane hydrophilicity.

Despite the above advantages (thermodynamic stability and hydrophilicity) of polymer blends, it is generally known that there is always a compromise in rejection and mechanical properties when increasing the hydrophilicity of a membrane. This usually results from the type of membrane morphology formation, typically revealed from the cross-section of the membrane. The morphology of a membrane plays a vital role in tailoring the mechanical strength of a membrane. It has been reported that the morphology of blended membrane that does not consist of macro-voids and finger-like structures shows more mechanical strength properties than when it does [23,24,28]. For example, Yang and Liu [23] reported finger-like structures sub-layer in the cross-section of a PAN/PVDF blended membrane, which depicts that as the PVDF content increases, the finger-like structures increased, consequently compromising the mechanical strength compared to those with smaller finger-like structures. Xu et al. [24] reported similar finger-like structures in PAN/PVDF to blend for both the pristine and modified membrane, however, the mechanical strengths were not reported. Although the presence of macro-voids and finger-like structure allows free movement of filtrate during filtration, nevertheless, when the mechanical strength is weak, it may result in failure of the membrane at high pressures [29].

Recently, inorganic nanomaterials such as zeolite, titanium dioxide, graphene oxide, carbon nanotubes, and many other nanomaterials are being considered to improve the mechanical strength and selectivity of polymeric membranes. Among these commonly used nanomaterials, the exceptional high elastic modulus, electrical, thermal, and tensile strength properties of multi-wall carbon nanotubes (MWCNT) have made MWCNT a more viable option for various membrane applications [30,31]. For instance, Arash et al. [32] studied the behavior of CNT on the mechanical strength of CNT reinforced poly(methyl methacrylate) (PMMA) composite membrane, the simulation result reveals that the modified membrane was 16 times stiffer than the pristine membrane and there was a significate increase in the strength of the modified membrane [32]. Majeed et al. [33] modified PAN UF membrane with MWCNT and results from the study showed an increase in tensile strength,

viscosity, and flux of the modified membrane. More so, Liu et al. [34] used carboxyl-functionalized MWCNT to modify the properties of the PVDF membrane and showed evidence of the improved antifouling performance of the modified membrane. Different studies have confirmed the outstanding performance of CNT in various applications including blood purification, dye separation, and water/alcohol separation [34–36]. Therefore, this study incorporates O-MWCNT into PAN/PVDF blend to boost the water permeabilities, rejection as well as mechanical strength of the finger-like structured membrane without compromise among these properties. To the best of our knowledge, this will be the first work documenting a breakthrough in the modification of PAN/PVDF blended membrane with a newly synthesized oxidized-MWCNT for oily wastewater separation.

The present study aims to enhance the properties of the PAN/PVDF blended membrane by using different concentrations of oxidized-MWCNT to modify the structural morphology of the blended membrane as well as increase the mechanical strength of the membrane. Consequently, this is expected to reduce or eliminate the trade-offs not only between the flux and rejection but also confer on the membrane's excellent mechanical strength and antifouling properties. The membranes were fabricated using the phase inversion method and the optimal function of the membranes was evaluated from the result of the pure water flux, bovine serum albumin (BSA), and oil rejection.

2. Materials and methods

2.1. Materials

PAN of average molecular weight (Mw) of 150,000 g/mol and PVDF (Solef®6020 670,000–700,000 Mw) were obtained from Shanghai Macklin B.O Chemical Co., Ltd., and Solvay (Shanghai) Co., Ltd., respectively. Polyvinyl pyrrolidone (PVP) K30, *N*,*N*-dimethylformamide (DMF), sodium dodecyl sulfate (SDS) were obtained from Sinopharm Chemical Reagent Co., Ltd., (China). Additionally, MWCNT (98% purity) was purchased from Beijing Deke Daojin Science and Technology, Co., Ltd., (China). BSA was purchased from Aladdin Industrial Company (China) and air compressor lubricating oil from Shengao Oil Co., Ltd., (China).

2.2. Synthesis and characterization of O-MWCNT

O-MWCNT were prepared via pretreatment of MWCNT in a mixed solution of HNO_3/H_2SO_4 (1:3, v/v) and refluxed at 70°C for 2 h. Thereafter, it was filtered and washed with distilled water until the pH was about 6 and then oven-dried at 80°C overnight. The resulting O-MWCNT nanoparticles were characterized via Fourier transform infrared spectroscopy (FTIR), X-ray diffraction (XRD), and surface area analyzer using Brunauer–Emmett–Teller (BET) method of nitrogen sorption at 77 K.

2.3. Membrane preparation

All membranes were fabricated using phase inversion and immersion precipitation method. The casting solution of the membranes consists of 15% polymer, 5% additive, and 80% solvent. However, the concentration of O-MWCNT added to the casting solution using the plus method is shown in Table 1. The ratio of the blended membrane (PAN:PVDF) used was 0.98:0.2, this was determined from the ΔH_m value obtained from the Schneier formula in Eq. (1).

$$\Delta H_m = \left\{ X_1 M_1 \rho_1 \left(\delta_1 - \delta_2\right)^2 \left(\frac{X_2}{\left(1 - X_2\right) M_2 \rho_2 + \left(1 - X_1\right) M_1 \rho_1} \right) \right\}^{1/2} \tag{1}$$

where M, ρ, and δ are the molecular weight of the monomer unit (g/mol), the polymer density (g/mol), and the solubility parameter of the polymer (cal/cm^3), respectively. Also, X_1 and X_2 are the mass fractions of the polymers, where the summation of X_1 and X_2 must be equal to 1. The casting solutions were prepared firstly by dissolving weighted percentage of O-MWCNT into DMAc solvent and then sonicated for 1 h. Thereafter, the polymer and additive were added to the resulting solutions and stirred thoroughly using a magnetic stirrer to achieve a homogenous mixture for about 24 h at 60°C. After the stirring procedure, the casting solutions were cooled at room temperature and degassed to get rid of air bubbles before casting. The solutions were casted on a non-woven fabric attached to a glass plate using a casting knife of 100 μm thickness, the resulting formation were immediately immersed in the coagulation bath at room temperature. Furthermore, all the membranes were kept in water for 24 h to eradicate the solvent and additive before testing the operation and characteristics of the membrane.

2.4. Oil–water emulsion preparation

The oil–water emulsion was prepared using 10:1:1,000 w/w of lubricating oil, SDS, and deionized water,

Table 1
Percentage composition of O-MWCNT/PAN/PVDF blended membrane

Membrane	PVP (wt.%)	PAN (wt.%)	PVDF (wt.%)	O-MWCNT (wt.%)	DMAc (wt.%)
M0	5	14.7	0.3	0	80.00
M1	5	14.7	0.3	0.01	80.00
M2	5	14.7	0.3	0.03	80.00
M3	5	14.7	0.3	0.05	80.00
M4	5	14.7	0.3	0.08	80.00
M5	5	14.7	0.3	0.1	80.00

and then stirred at 1,500 rpm for 3 h to obtain a surfactant stabilized oil emulsion.

2.5. Membrane characterization

2.5.1. Morphology of the membrane

Field emission scanning electronic microscopy (SEM S-4800, HITACHI, Japan), was used at 5 kV and 10 μA to investigate the surface and cross-sectional morphology of the membrane. FTIR and X-ray photoelectron spectroscopy (XPS, ESCALAB 250XI, Thermo, USA) was used to investigate the functional groups and the different chemical bonds present in the membrane, respectively. Also, atomic force microscopy (AFM, Dimension Icon, Bruker, USA) was used to investigate the structure and roughness of the membrane surface.

2.5.2. Hydrophilicity and porosity of the membrane

The hydrophilicity of the membrane was determined by measuring the contact angle of the membrane using a contact angle analyzer (DSA100, KRUSS, German). Five different spots were recorded on each of the membrane and the average value of the angles was reported.

The porosity (ε) of the membrane was calculated using dry–wet weight equation as shown in Eq. (2):

$$\varepsilon(\%) = \frac{W_1 - W_2}{\rho_w t A} \times 100 \tag{2}$$

where W_1, W_2, t, and A represent the wet weight (g), dry weight (g), thickness (cm), and area (cm^2) of the membrane, respectively, while ρ_w represents the density of water (g/cm^3). In addition, the mean pore radius (r_m) was derived using Eq. (3):

$$r_m = \sqrt{\frac{(2.9 - 1.75\varepsilon) \times 8\mu t Q}{\varepsilon \times A \times P}} \tag{3}$$

where μ, Q, and P are the viscosity of water (8.9×10^{-4} Pas), volume permeates pure water per unit time (m^3/s) and the operation pressure (MPa).

2.6. Operational test

A dead-end filtration cell was used to evaluate the pure water flux of the membrane with an effective area of 13.16 cm^2. The membranes were initially compacted under deionized water at 0.15 MPa for 30 min to obtain a steady flux, after which the pressure was reduced to 0.1 MPa and the permeate was measured. The flux was evaluated using Eq. (4):

$$J_1 = \frac{V}{A \times T} \tag{4}$$

where J_1, V, A, and T represent the flux of the membrane (L/m^{2}h), volume of the permeate (L), effective area of the filtration cell (m^2), and the time taken for permeation (h).

BSA solution of 1 g/L and the prepared oil–water emulsion was used to evaluate the rejection performance of the membrane. The difference in the feed concentration and the permeate concentration for both BSA and oil–water emulsion solution was evaluated using a UV spectrophotometer at a wavelength of 280 and 260 nm, respectively. The rejection performance was calculated using Eq. (5):

$$R = \left(1 - \frac{C_p}{C_f}\right) \times 100\% \tag{5}$$

where R is the rejection percentage, C_p is the concentration of the permeate, and C_f is the concentration of the feed.

2.7. Antifouling performance of membrane

The antifouling properties of the membrane were analyzed using the flux recovery before and after the separation process. Pure water flux was initially carried out to obtain the flux (J_1) before separation, and then the BSA solution was permeated through the membrane to obtain another flux (J_0). Afterwards, the membranes were washed with deionized water, and a new pure water flux (J_2) was obtained. This whole process was also carried out with respect to oil–water separation. The flux recovery ratio (FRR), reversible fouling ratio (R_r), and the irreversible fouling ratio (R_{ir}) of the membrane were calculated using Eqs. (6)–(8), respectively:

$$\text{FRR} = \left(\frac{J_2}{J_1}\right) \times 100 \tag{6}$$

$$R_r = \left(\frac{J_2 - J_0}{J_1}\right) \times 100 \tag{7}$$

$$R_{ir} = \left(\frac{J_1 - J_2}{J_1}\right) \times 100 \tag{8}$$

Furthermore, some fouling parameters were used to examine the fouling process of the membrane. These parameters include pore resistance (R_f) resulting from pore blockage, intrinsic resistance (R_m) which is due to the membrane thickness and pore size, and cake resistance (R_c) resulting from the cake layer on the membrane surface. Eqs. (9)–(11) were applied to evaluate these parameters:

$$R_f = \left(\frac{\Delta P}{\mu J_2}\right) - R_m \tag{9}$$

$$R_m = \left(\frac{\Delta P}{\mu J_1}\right) \tag{10}$$

$$R_c = \left(\frac{\Delta P}{\mu J_2}\right) - R_m \tag{11}$$

2.8. Mechanical strength

The mechanical strength of the membrane was studied using a universal testing machine, and was evaluated by measuring the tensile strength and percentage of elongation of the membrane. The membranes were placed within the sample holder of the machine and the obtained readings were recorded at a speed of 1 cm/min.

3. Results and discussion

3.1. Characteristic properties of O-MWCNTs

Fig. 1 shows the XRD, FTIR, N_2-adsorption isotherm, and the corresponding pore-size-distribution calculated from the density-functional theory (DFT) method. As shown in Fig. 1a, the XRD pattern of the O-MWCNTs shows a major peak at 2θ = 25.74° corresponding to the (002) reflection, which indicates the hexagonal graphitic carbon structure of O-MWCNT. Furthermore, as illustrated in Fig. 1b, the FTIR spectra examination reveals the oxidation result of the acid treatment on the MWCNT by the presence of hydrophilic function group OH at characteristic band 3,450 cm^{-1}, as well as 1,650 and 1,060 cm^{-1} indicating C=O and C–O vibrations, respectively. The N_2-adsorption isotherm of the O-MWCNT illustrated in Fig. 1c reveals a type IV isotherm having a hysteresis loop at $0.5 < P/P_0 < 1.0$. This indicates the presence of mesoporous structures which also correspond to the result of the pore size distribution in Fig. 1d.

3.2. Compatibility of PAN/PVDF polymer blend

A major drawback of the polymer blend is the incompatibility between individual polymers. Generally, when polymers are incompatible, it indicates the absence of definite interaction between the polymers [37,38]. Consequently, the miscibility of polymer is basically dependent on the molecular interaction due to the dispersive force, dipolar force, and hydrogen bond [39]. The compatibility between PAN and PVDF was calculated using the Schneier formula in Eq. (1). The polymer parameters used for this analysis are indicated in Table 2, while the resulting ΔH_m values of different PAN/PVDF ratios are shown in Fig. 2. As shown in Fig. 2, the ΔH_m value was influenced by the composition of PAN/PVDF. When the weight ratio of PAN/PVDF was more than 0.98:0.02, the ΔH_m was $>10 \times 10^{-3}$ cal/mol and vice versa. This indicated that PAN and PVDF are compatible at a weight ratio of 0.98:0.02 or less, and are incompatible at a greater weight ratio mix. The incompatibility between PAN and PVDF illustrated the diverse behavior

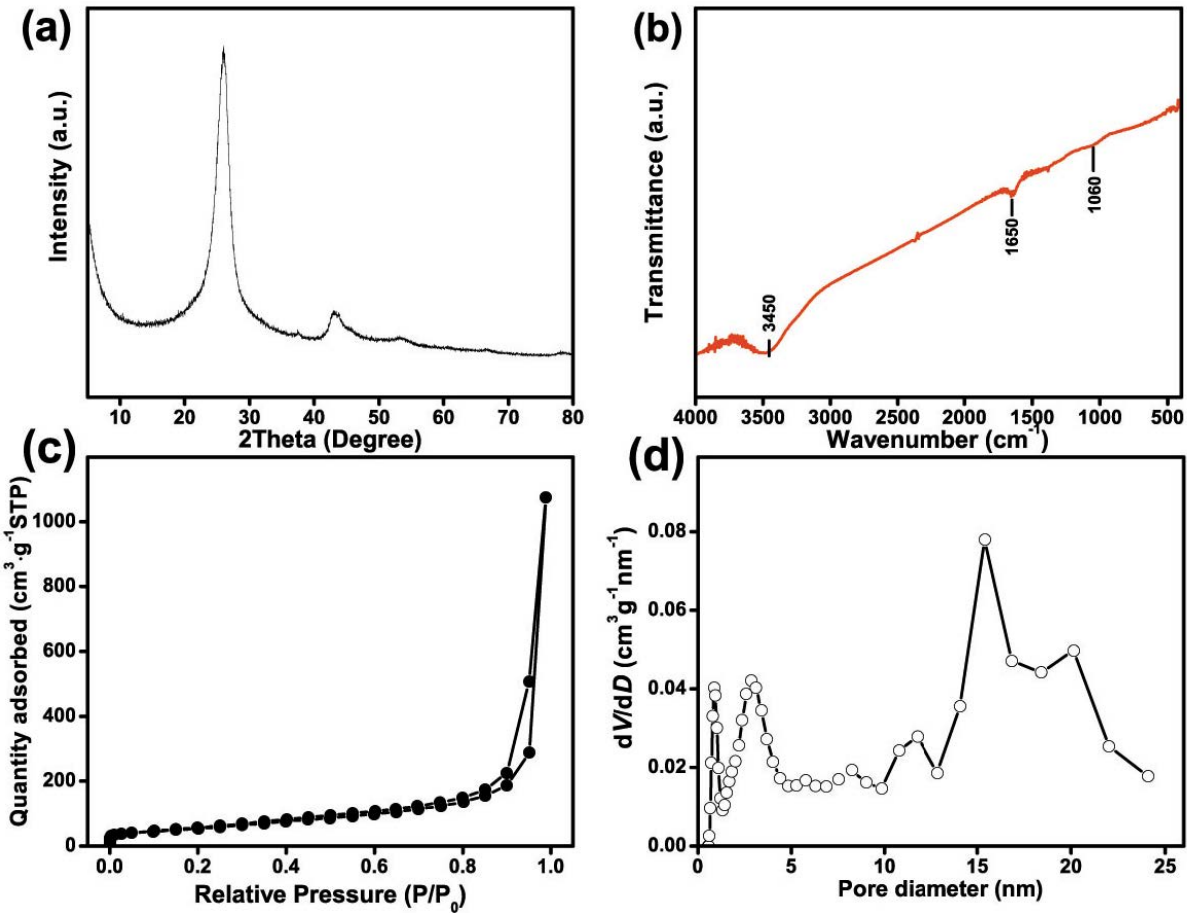

Fig. 1. (a) XRD, (b) IR, (c) N_2-adsorption isotherm, and (d) the corresponding pore-size-distribution calculated from the DFT method.

Table 2
Density, molecular weight, and solubility parameter of PAN and PVDF polymer

Polymer	PAN	PVDF
Density	1.17	1.6
Molecular weight (g/mol)	53.06	64.03
Solubility $(cal/cm^3)^{1/2}$	12.89	7.63

of strong repulsive force between the two hydrophobic macromolecules materials. More so, the hydrophobic PVDF macromolecules were dominated by the hydrophobic PAN matrixes, which put a strain on the connectivity of the two polymers. Consequently, PAN/PVDF polymer blend is partially compatible with each other, which was similarly reported by Xiuli et al. [28]. Nevertheless, at a very small weight ratio of PVDF, the blended polymer showed good miscibility. As a result, 0.98:0.02 weight ratio of PAN/PVDF was considered for the fabrication of the membrane.

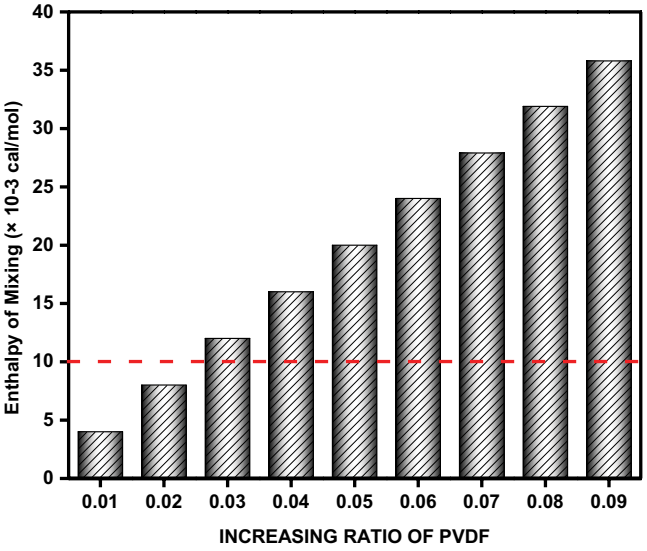

Fig. 2. Enthalpy of mixing different PAN/PVDF ratios.

3.3. Characterization of O-MWCNT/PAN/PVDF

3.3.1. Membrane morphology

SEM was carried out to visualize the morphology of the membranes. The surface and cross-section morphology of the blended membrane with increasing O-MWCNT loading are portrayed in Fig. 3. As revealed on the surface morphology ($M0^a$–$M5^a$), the PAN/PVDF membrane was free of O-MWCNT, while the modified membranes showed increasing light spot with increasing loading of O-MWCNT. Besides, O-MWCNT spots were not clustered at a particular point, indicating a well-distributed O-MWCNT for all the modified membranes. A similar observation of light spots was reported by other researchers [39,40]. As illustrated from the cross-sectional view in Fig. 3 ($M0^b$–$M5^b$), all membranes exhibited asymmetric finger-like structure in the cross-sectional morphology. The permeation and rejection of the solution are based on the top layer of the membrane while the sublayer functions as the supportive layer [35,41]. The addition of O-MWCNT into the blended membrane did not change the mechanism formation of the membrane.

Although, the addition of O-MWCNT increased the size of the finger-like structure, which explains the increase in the flux of the modified membrane and this might have emerged from the fusion of vanishing macro-voids resulting from the increase in solution viscosity [33]. However, the large finger-like structure reduces after a further increase in O-MWCNT, this might also be the reason for the decrease in flux after the peak flux in M3 as explained in section 3.5 (operation performance). A closer study on the cross-sectional walls reveals a denser wire-like structure ($M0^c$–$M5^c$) as the O-MWCNT increases which might be responsible for the increase in the mechanical strength of the membrane.

Furthermore, the membrane surface roughness was examined using AFM and the result are illustrated in Fig. 4. It was observed that the roughness parameter (average roughness R_a) increased with an increase in the O-MWCNT from 30.1 to 61.1 nm. This is because the nanofillers moved impulsively into the blended membrane interface, thus producing coarse membrane surface. The introduction of roughness and hierarchical structure to the membrane surface generally improves the hydrophilicity of the membrane, thereby enhancing the fluxes of the membrane [42].

3.3.2. FTIR and XPS analysis

FTIR and XPS were used to examine the functional groups and chemical bonds on the surface of the membranes. The functional groups of all membranes obtained from the FTIR spectra are shown in Fig. 5. The modified membranes (M1–M5) showed a small peak of carboxylic acid group C=O at 1,731 cm^{-1} and a stretching O–H group at 3,444 cm^{-1}, these peaks indicated the presence of O-MWCNT in the blended membrane. All the membranes displayed common peaks of PAN C≡N (nitrile) at 2,234 cm^{-1}, small PVDF C–F at 1,291 cm^{-1}, stretching C–H at 2,939.63 cm^{-1}, and C–O at 1,072 cm^{-1}. Marie et al. [43] reported that a shift in the C≡N peak could be as a result of the interaction between C≡N and O–H bond [43]. Although, a slight shift was observed at the C≡N peak in all modified membranes, most especially in the M5 membrane with the highest O-MWCNT concentration. Nevertheless, this shift cannot fully justify the hydrogen bonding between C≡N and O–H bond. In order to understand the interactions between the bonds in the blended membrane and the O-MWCNT, further investigation was carried out using XPS analysis.

Fig. 6 shows the schematic hydrogen bonds between the polymers and nanofillers, as well as the XPS results for M0 and M5 membranes. As depicted in Fig. 6b, common peaks of the major chemical component were recorded at a binding energy of 284.80, 397.04, 530.05, and 685.01 eV for C1s, N1s, O1s, and F1s, respectively. It was also observed that the intensity of oxygen and the O/C atomic ratio increased in M5 compared to M0. This suggested the presence of O-MWCNT in the modified membrane. Further studies on the interaction of the oxygen bonds for O1s core-level spectrum are

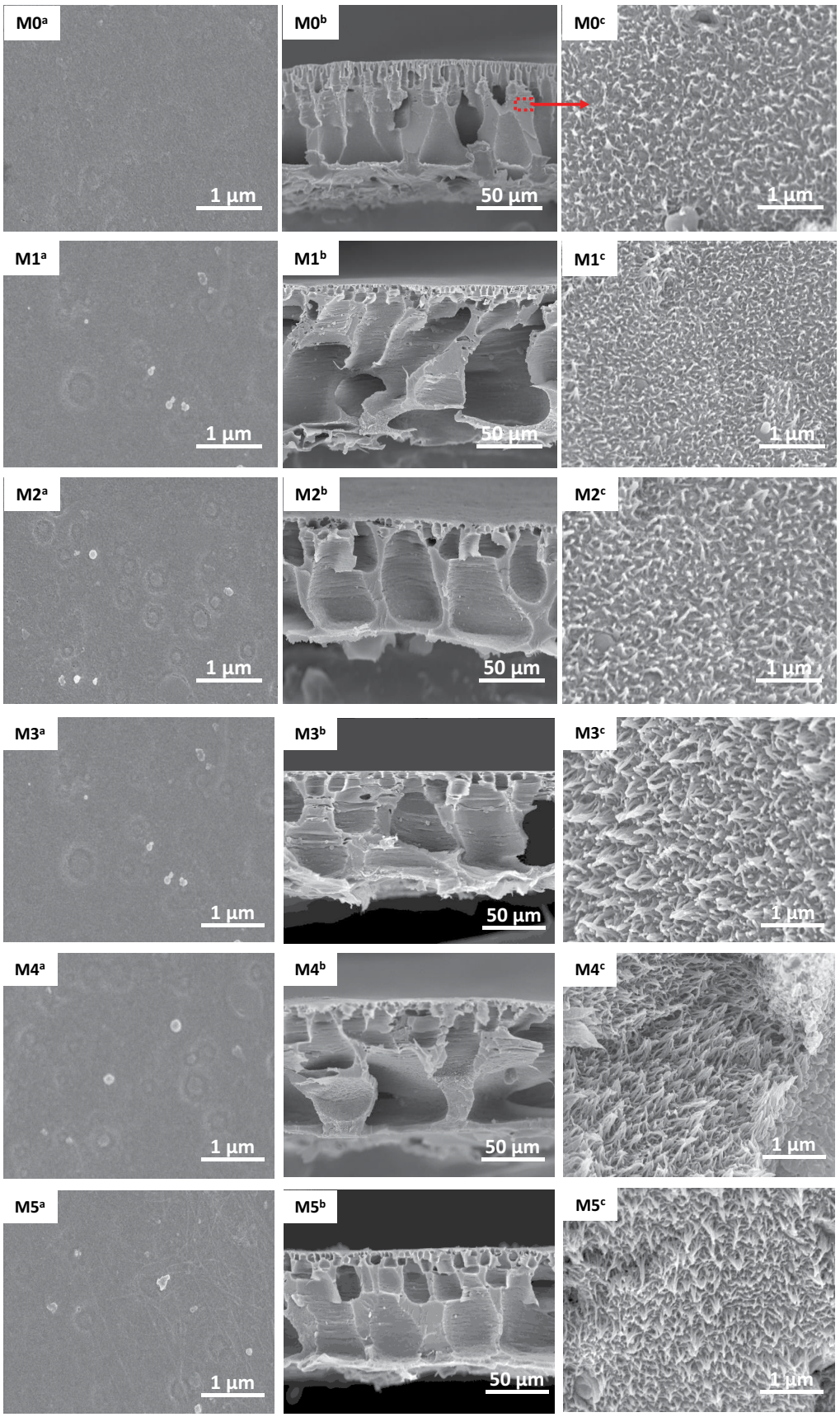

Fig. 3. SEM image of surface[a] and cross-sectional[b,c] morphology of blended membrane for M0–M5.

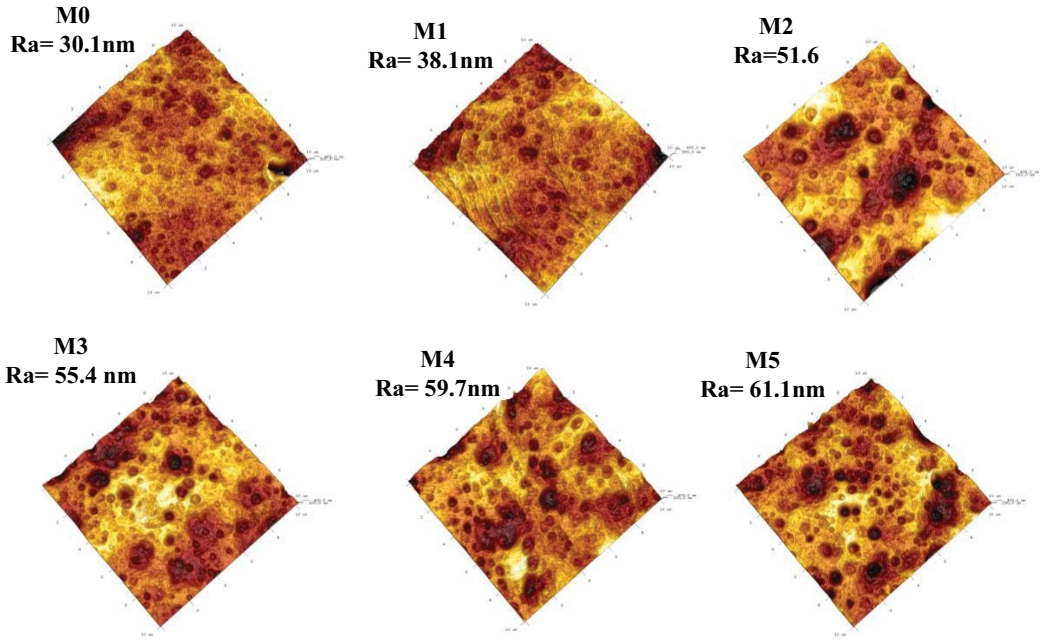

Fig. 4. AFM image of the fabricated membrane M0–M5.

described in Figs. 6c and d. The core-level spectrum for M0 could be fitted into two curves representing C–O and C=O, while M5 could be fitted into four curves representing C=O, C–O, [NH]COOH, and OH bonds. These addition bonds in M5 were based on the interaction between O-MWCNT and PAN/PVDF. Besides, these additional bonds could be responsible for the shift observed at the C≡N peak in FTIR analysis and the hydrophilicity of the modified membrane.

3.4. Porosity and contact angle

As shown in Fig. 7, the contact angle of the membrane decreased at the addition of the O-MWCNT from 65° to 60° at 0.01% O-MWCNT and further to 52° at 0.1% O-MWCNT. This implies that the surface hydrophilicity of the membrane increases with an increase in O-MWCNT resulting in the enhancement of the antifouling properties. This is due to the OH group introduced into the blended membrane by the O-MWCNT. This result is similar to other researchers' outcomes [15,33]. Besides, because of the electronegativity of H and N atoms that led to the polar behavior of N–H bonds, the hydrogen bonding reaction can absorb water molecules resulting into enhanced hydrophilicity of the membrane [44].

Fig. 8 illustrates the porosity and the mean pore size of the fabricated membranes. It was deduced that the bulk porosity and the mean pore radius of the membrane increase with the addition of O-MWCNT. Although, the mean pore size deceased with further increase in the O-MWCNT content in M3, M4, and M5, which could be attributed to the partial cluster of the nanotubes at higher O-MWCNT loading. The increase in porosity substantiated the initial increase in the water permeation while the further decrease in the mean pore size validated the reduction in the water permeation at corresponding

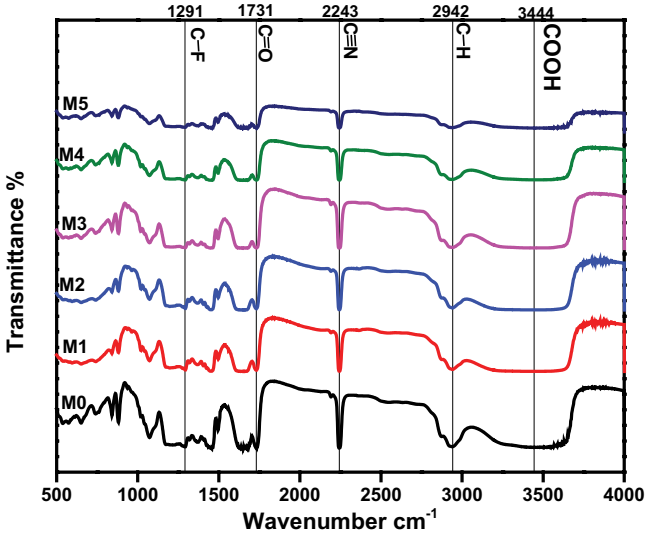

Fig. 5. FTIR spectra of fabricated membrane M0–M5.

membrane M3, M2, and M5. Nevertheless, all modified membranes showed higher hydrophilicity than the unmodified membrane and eventually, the membranes with the bigger pore size have higher fluxes. This implies that the pore size has more influence than surface hydrophilicity.

3.5. Operation performance

3.5.1. Pure water flux and BSA rejection

Fig. 9 exhibits the water flux and BSA rejection of all the prepared membranes. The flux increased in all the modified membrane compared to the pristine membrane with M2 (0.03% O-MWCNT) having the highest flux of

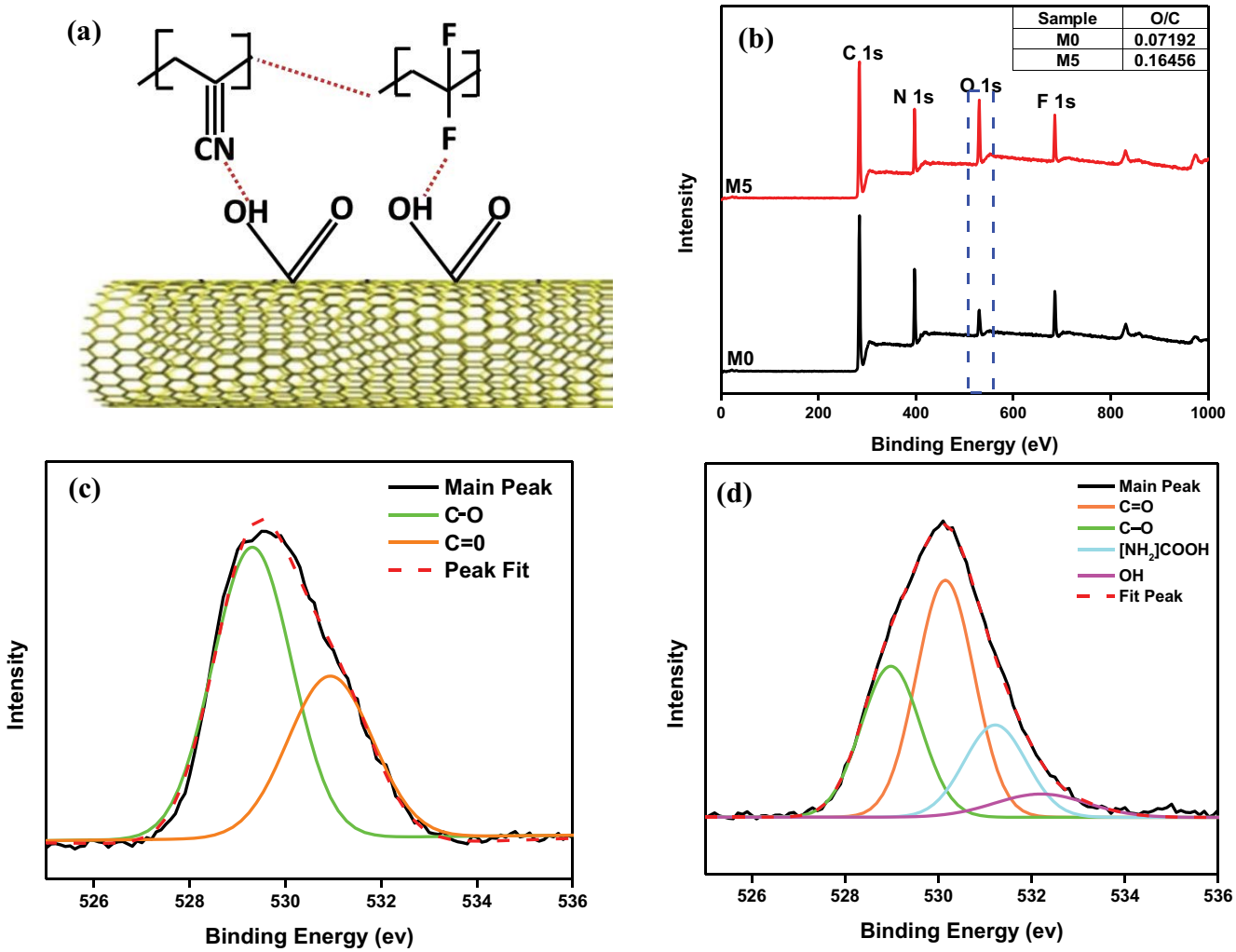

Fig. 6. (a) Hydrogen bonds between the polymer and O-MWCNT, (b) survey XPS spectra and the O/C ratio of M0 and M5, (c) O1s core-level spectra of M0, and (d) O1s core level spectra of M5.

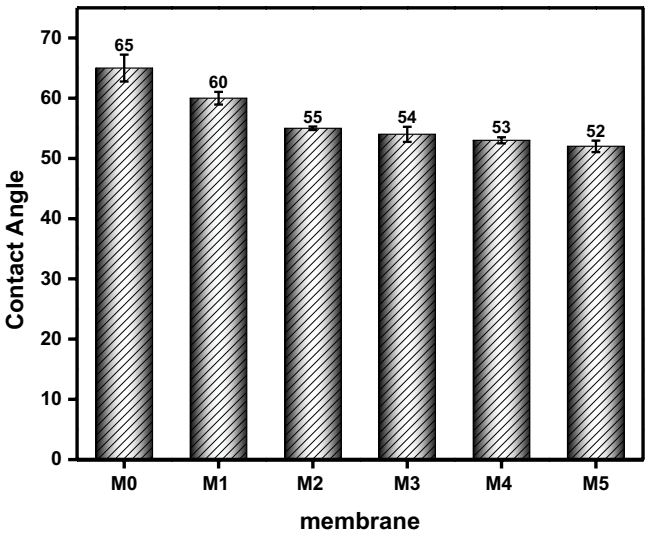

Fig. 7. Contact angle of the fabricated membranes M0–M5.

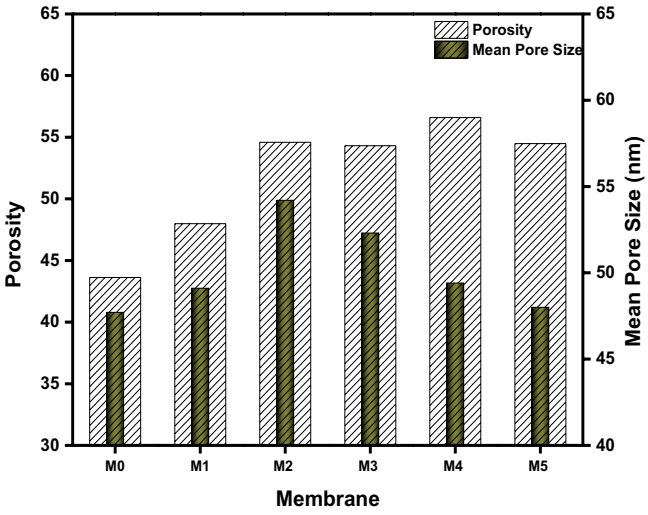

Fig. 8. Porosity and mean pore size fabricated membranes M0–M5.

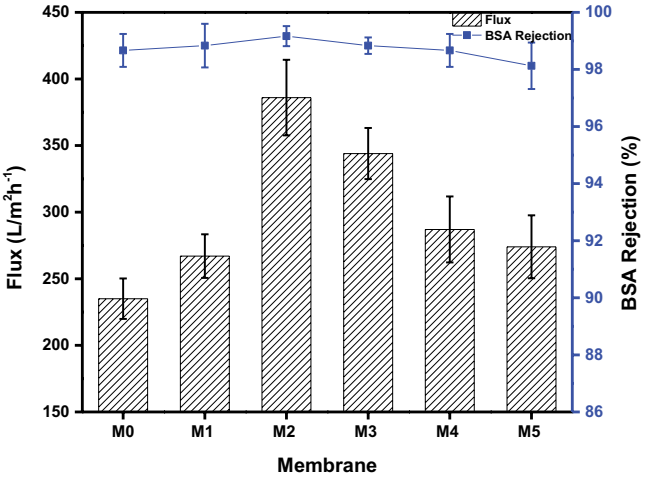

Fig. 9. Pure water flux and BSA rejection of the fabricated membranes M0–M5.

about 386 L/m² h (65% increase). The initial increase in flux in M1 and M2 was due to the increase in porosity, hydrophilicity, and pore size of the membranes. However, the decrease in flux in M3, M4, and M5 was by dint of the decrease in mean pore size and the membrane finger-like structure, as explained in sections 3.3 (characterization of O-MWCNT/PAN/PVDF) and 3.4 (porosity and contact angle), which plays an indelible role in the flux decrease of these membranes. At a lower concentration of O-MWCNT, the hydrophilic nature of O-MWCNT enhanced the interchange between solvent and non-solvent during the phase inversion process which resulted into the formation of larger pore sizes. Conversely, at higher concentrations, there was an increase in the viscosity of the casting solution, which interferes with the phase separation process [34]. This led to the formation of smaller pore sizes resulting in to decrease in water flux. The percentage of the BSA rejection is also illustrated in Fig. 9. It was observed that all membranes have a rejection of over 97%. Although statistically, no significate difference between the membrane rejection at $p > 0.05$, however, the modified membrane with 0.03% O-MWCNT has the highest rejection of about 99%. This suggests that the addition of O-MWCNT into the blended membrane is not detrimental to the improvement in flux with the solute rejection. An ultrafiltration membrane with reasonable improved flux, small pore size, high rejection, and porosity is more suitable for membrane operations [15]. More so, providing a balance between the trade-off of permeability and selectivity and this could be found in the modified membrane.

3.5.2. Oil and water separation

The efficiency of the prepared membrane was tested through the separation of lubricating oil and water, and the result are illustrated in Figs. 10a–d. The result revealed that the presence of O-MWCNT in the blended membrane did not only improve the water flux as shown in Fig. 9, but also enhanced the oil–water permeate flux from 61 to 84 L/m² h as well as the oil rejection as indicated in Fig. 10a. The increase in permeate flux could be attributed to the hydrophilic nature of O-MWCNT while the improvement in rejection could be as a result of the anti-oil adhesion properties of the nanotube. Generally, lubricating oil has a high viscosity and density which could limit the movement of oil and water mixture through the membrane, however, the presence of O-MWCNT aids the movement of permeate through the membrane by increasing the flux to a reasonable extent. Moreover, the hydrodynamic shearing force between the oil droplet and the modified membrane allows the oil droplets to go back to the concentrated feed stream, consequently, improving the permeate flux. The further decrease in permeate flux could be ascribed to the decrease in the pore size of the membranes.

Fig. 10b shows the efficiency of the membrane with the optimal performance (M2, 0.03% O-MWCNT). The membrane shows excellent stability and consistency in the separation of oil over a 28-cycle separation process in which each cycle takes a duration of 3 h (Fig. 10b). More so, the membrane maintained its rejection efficiency which is more than 98%, and without an obvious decrease in the permeate flux throughout the 84 h separation process. This is worth noting that the oil droplet was reduced to less than 0.5 μm after separation, as shown in Fig 10c. In addition, Fig. 10d shows the photographic image of the oil and water mixture before and after separation. As revealed in this Fig. 10, the obtained permeate was translucent without noticeable droplets, while the feed mixture was milky white. This suggests an excellent separation performance of the modified membrane.

3.5.3. Antifouling properties

Fig. 11 illustrates the time-dependent flux for fouling evaluation of the membranes. This experiment comprises of three stages, stages 1 and 3 was for the pure water filtration while stage 2 was for the oil and water filtration. As shown in Fig. 11, the flux recovery for M0 drops from 245 to 180 L/m² h, whereas, the recovery flux of the membrane with the highest O-MWCNT drops slightly from 279 to 270 L/m² h. This indicated the excellent antifouling properties of O-MWCNT. The basic parameter that is usually utilized to explain antifouling property is FRR. To further understand the antifouling properties of the membranes, the FRR and fouling resistance were evaluated for both BSA and oil separation, and are illustrated in Fig. 12. The FRR increased with an increase in the O-MWCNT content to about 96% and 93% for oil and BSA separation, respectively, compared to the pristine membrane of 71% (Figs. 12a and b). More so, the improvement in the FRR in the modified membrane could be linked to the increased in the hydrophilicity as discussed in section 3.3 (characterization of O-MWCNT/PAN/PVDF) which agreed with most literatures [34,41,45,46].

The result of the fouling resistance shows that irreversible fouling ratio decreases with the addition of the O-MWCNT while the reversible fouling ratio increases for both oil and BSA separation as illustrated in Figs. 12c and d, respectively. Also, the fact that the pure water flux was easily recovered in Fig. 11 and no obvious decrease in

the permeate flux after each separation cycle in Fig. 10b, indicates that the modified membrane was less liable to irreversible fouling. Furthermore, fouling parameters such as intrinsic resistance, pore resistance, and cake resistance were used to examine the fouling process of the fabricated membrane, and the results are shown in Fig. 13. As illustrated in Fig. 13, the intrinsic resistance contributes to the bulk of the resistance of the pristine membrane, which was responsible for the low flux in the pristine membrane. However, the presence of the O-MWCNT did not only reduce this type of resistance but also the other forms of resistance (cake and pore resistance). Consequently, the total fouling resistance of the membrane was significantly reduced.

3.6. Mechanical strength

A major reason for considering oxidized multi-wall carbon nano-tubes as strengthen nanofillers in a composite membrane is because they function as stress absorbers when external loads are exacted to the membrane [15,47]. Mechanical test was carried out in terms of tensile strength and percentage of elongation at break to evaluate the mechanical properties of the membranes. In addition, viscosity measurement of the membrane casting solutions was used to justified the mechanical strength of the membrane. This is because an increase in the viscosity of the casting solution can influence the decrease in the diffusion between the solvent and non-solvent phase inversion component. This process can lead to the delay in the exchange of these components which further suppresses the macro-voids in the membrane and subsequently improves the mechanical strength [33,48]. Fig. 14 shows the viscosity measurement of the casting solution and the mechanical strength

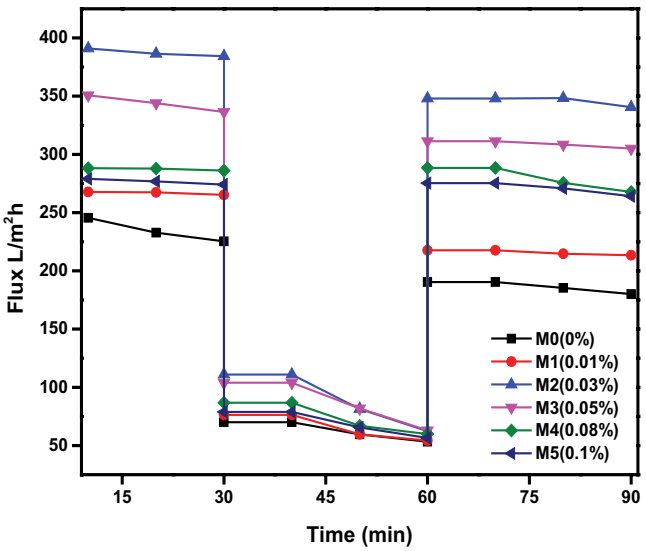

Fig. 11. Time-dependent flux for antifouling examination.

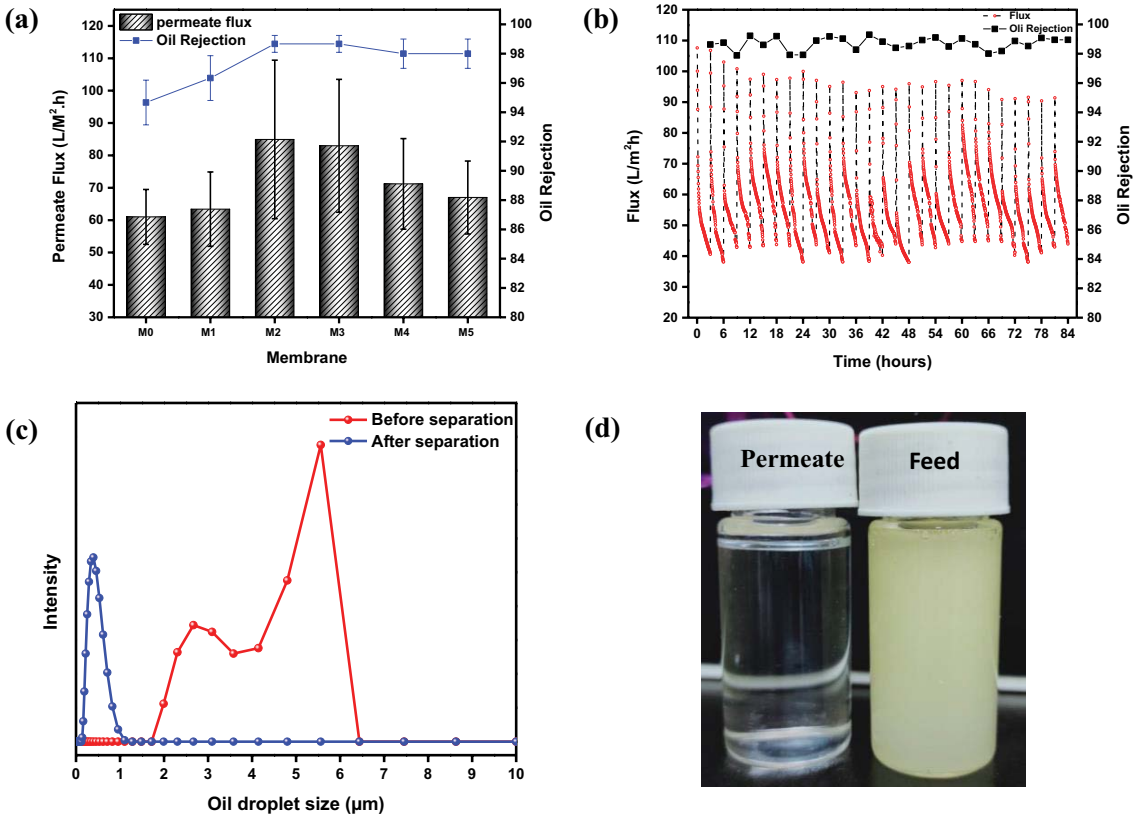

Fig. 10. (a) Oil permeate and rejection for membranes M0–M5, (b) 28 cycle oil separation process, (c) oil droplet before and after separation, and (d) pictorial view of the feed and permeate before and after separation.

of the membranes. The viscosity of the membrane increases with an increase in O-MWCNT at different temperatures (35°C–60°C) as depicted in Fig. 14a. This increase could be due to the several interactions of hydrogen bonds between the polymers and O-MWCNT, and also, between O-MWCNT and O-MWCNT. Consequently, an increase in O-MWCNT content would increase the hydrogen bonds in the modified membranes. These bonds constrain the movement of the polymer chain, therefore increases the viscosity of the casting solution. Subsequently, improves the mechanical strength of the modified membranes. It was also discovered that as the temperature increases, the viscosity decreases. This could have resulted from the increase in the kinetic energy based on the high temperature leading to the free movement of the polymer chain. Fig. 14b shows the tensile strength and the percentage of elongation at the breakpoint of the membrane. It was observed that the presence of the O-MWCNT in the blended membrane gradually increased the tensile strength and the elongation percentage of the membrane from 4.11 MPa at 13.33% to 5.94 MPa at 16.02% elongation. This increase affirms the

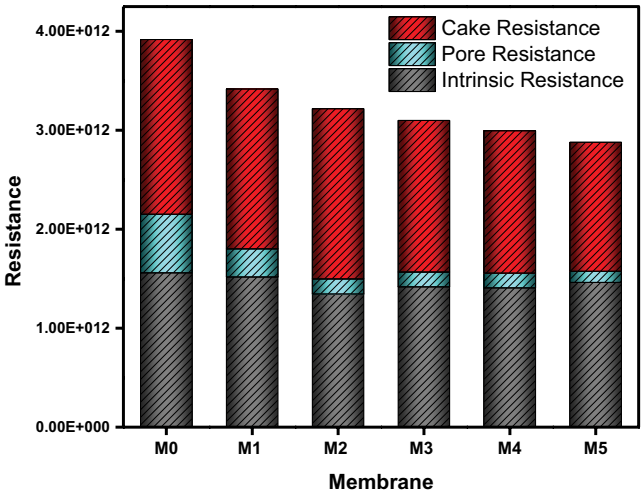

Fig. 13. Fouling parameters for membranes M0–M5.

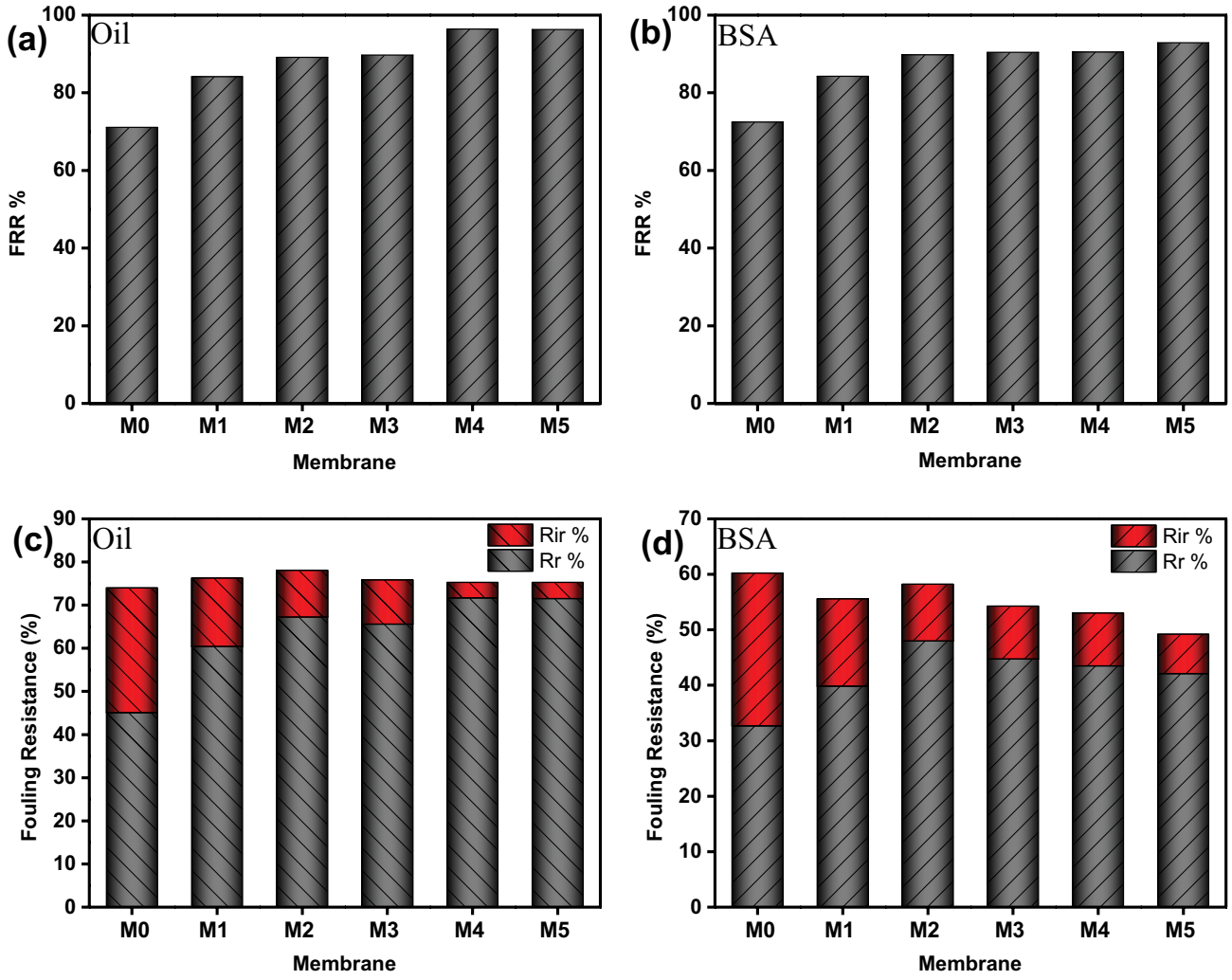

Fig. 12. Flux recovery ratio for (a) oil separation and (b) BSA separation; fouling resistance for (c) oil separation and (d) BSA separation.

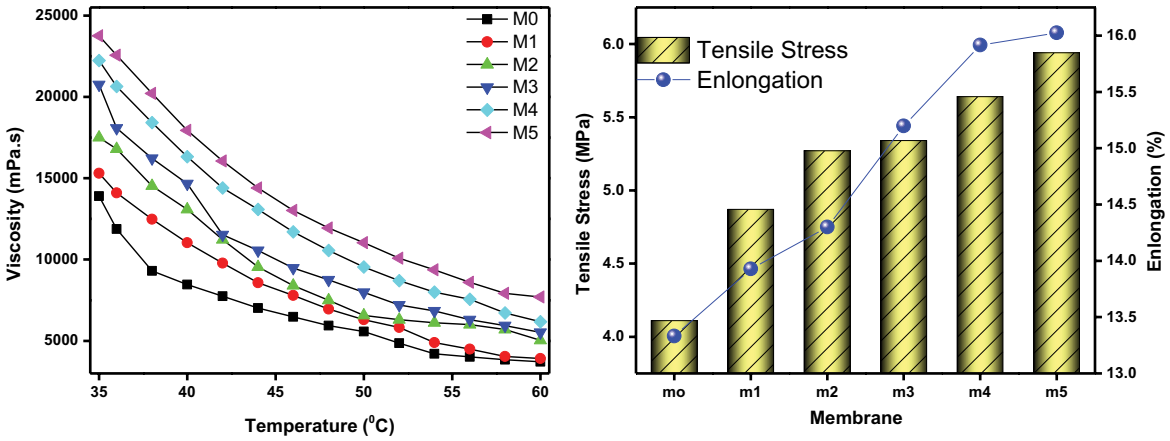

Fig. 14. (a) Viscosity measurement of the casting solution at different O-MWCNT loading and (b) mechanical strength of the membrane M0–M5.

strong interaction of the hydrogen bonds and the sufficient bond interactions between the nanofiller and the membrane components. Consequently, when stress or loads are applied to the membrane, some of the loads would be transferred to the filler, which increases the life span of the membrane. More so, the increase in the elongation indicated that the modified membranes are capable of resisting changes of shapes without the development of cracks.

4. Conclusion

O-MWCNT/PAN/PVDF ultrafiltration membrane with enhanced properties was successfully fabricated using the phase inversion process. The effects of O-MWCNT on improvements of the physical and chemical morphology of the PAN/PVDF blended membrane were investigated, and the operational performance of the membrane was evaluated. The results revealed that the presence of the O-MWCNT in the blended membrane increased the flux up to 65% compared to the pristine membrane without having an adverse effect on the oil and BSA rejection, consequently, creating a balance between the membrane trade-off for permeability and rejection. Furthermore, the O-MWCNT/PAN/PVDF membrane showed improved antifouling properties and maintained stability and consistency in flux and oil rejection after 84 h of separation. Also, the addition of O-MWCNT showed an increase in viscosity of the casting solution which signifies a uniform distribution of the O-MWCNT and the reaction of hydrogen bonds between the polymers and the nanofillers, hence improving the mechanical strength of the membrane. Although the structural morphology showed a finger-like structure, nevertheless the addition of the nanofillers helps to improve the tensile strength and the elongation percentage of the membrane. Overall, the fabricated O-MWCNT/PAN/PVDF membrane exhibited outstanding and promising properties, which are of great benefit in the field of emulsified oily wastewater treatment.

Acknowledgments

This work was supported by grants from the Bureau of International Cooperation (132C35KYSB20160018), the Chinese Academy of Sciences (CAS), and the Chinese Academy of Sciences-The World Academy of Sciences (CAS-TWAS) president's fellowship program for developing countries. We acknowledge Hongyun Ren and Zhen Xu at the Center of Analysis and Measurement from Institute of Urban Environment, CAS, for the TEM and XPS measurement, respectively, also Danmei Pan from Fujian Institute of Research on the Structure, CAS for the AFM test.

References

[1] Y. Sun, C. Zhu, H. Zheng, W. Sun, Y. Xu, X. Xiao, Z. You, C. Liu, Characterization and coagulation behavior of polymeric aluminum ferric silicate for high-concentration oily wastewater treatment, Chem. Eng. Res. Des., 119 (2017) 23–32.
[2] N.H. Ismail, W.N.W. Salleh, A.F. Ismail, H. Hasbullah, N. Yusof, F. Aziz, J. Jaafar, Hydrophilic polymer-based membrane for oily wastewater treatment: a review, Sep. Purif. Technol., 233 (2020) 116007 (1–18), doi: 10.1016/j.seppur.2019.116007.
[3] R.H. Hesas, M.S. Baei, H. Rostami, J. Gardy, A. Hassanpour, An investigation on the capability of magnetically separable Fe_3O_4/mordenite zeolite for refinery oily wastewater purification, J. Environ. Manage., 241 (2019) 525–534.
[4] A.A. Aly, Y.N. Hasan, A.S. Al-Farraj, Olive mill wastewater treatment using a simple zeolite-based low-cost method, J. Environ. Manage., 145 (2014) 341–348.
[5] Y. Fan, S. Simon, J. Sjöblom, Chemical destabilization of crude oil emulsions: effect of nonionic surfactants as emulsion inhibitors, Energy Fuels, 23 (2009) 4575–4583.
[6] L.C. Gobbi, I.L. Nascimento, E.P. Muniz, S.M. Rocha, P.S. Porto, Electrocoagulation with polarity switch for fast oil removal from oil in water emulsions, J. Environ. Manage., 213 (2018) 119–125.
[7] Y. Peng, F. Guo, Q. Wen, F. Yang, Z. Guo, A novel polyacrylonitrile membrane with a high flux for emulsified oil/water separation, Sep. Purif. Technol., 184 (2017) 72–78.
[8] C. Chen, B. Chen, Graphene oxide coated meshes with stable underwater superoleophobicity and anti-oil-fouling property for highly efficient oil/water separation, Sci. Total Environ., 696 (2019) 133777 (1–8), doi: 10.1016/j.scitotenv.2019.133777.
[9] M. Padaki, R. Surya Misdan, A. Moslehyani, M.A. Kassim, N. Hilal, A.F. Ismail, Membrane technology enhancement in oil–water separation. A review, Desalination, 357 (2015) 197–207.
[10] C. Zhou, J. Cheng, K. Hou, A. Zhao, P. Pi, X. Wen, S. Xu, Superhydrophilic and underwater superoleophobic titania nanowires surface for oil repellency and oil/water separation, Chem. Eng. J., 301 (2016) 249–256.
[11] F. Zhang, S. Gao, Y. Zhu, J. Jin, Alkaline-induced superhydrophilic/underwater superoleophobic polyacrylonitrile membranes

with ultralow oil-adhesion for high-efficient oil/water separation, J. Membr. Sci., 513 (2016) 67–73.
[12] J. Zhang X. Pan, Q. Xue, D. He, L. Zhu, Q. Guo, Antifouling hydrolyzed polyacrylonitrile/graphene oxide membrane with spindle-knotted structure for highly effective separation of oil-water emulsion, J. Membr. Sci., 532 (2017) 38–46.
[13] E.N. Tummons, V.V. Tarabara, J.W. Chew, A.G. Fane, Behavior of oil droplets at the membrane surface during crossflow microfiltration of oil–water emulsions, J. Membr. Sci., 500 (2016) 211–224.
[14] O.K. Abass, F. Fang, M. Zhou, K. Zhang, Integrated interrogation of causes of membrane fouling in a pilot-scale anoxic-oxic membrane bioreactor treating oil refinery wastewater, Sci. Total Environ., 642 (2018) 77–89.
[15] N.N. Gumbi, M. Hu, B.B. Mamba, J. Li, E.N. Nxumalo, Macrovoid-free PES/SPSf/O-MWCNT ultrafiltration membranes with improved mechanical strength, antifouling and antibacterial properties, J. Membr. Sci., 566 (2018) 288–300.
[16] A. Tiraferri, Y. Kang, E.P. Giannelis, M. Elimelech, Superhydrophilic thin-film composite forward osmosis membranes for organic fouling control: fouling behavior and antifouling mechanisms, Environ. Sci. Technol., 46 (2012) 11135–11144.
[17] S. Li, Z. Cui, L. Zhang, B. He, J. Li, The effect of sulfonated polysulfone on the compatibility and structure of polyethersulfone-based blend membranes, J. Membr. Sci., 513 (2016) 1–11.
[18] D. Rana, B.M. Mandal, S.N. Bhattacharyya, Analogue calorimetry of polymer blends: poly(styrene-co-acrylonitrile) and poly(phenyl acrylate) or poly(vinyl benzoate), Polymer, 37 (1996) 2439–2443.
[19] D. Rana, B.M. Mandal, S.N. Bhattacharyya, Analogue calorimetric studies of blends of poly(vinyl ester) and polyacrylates, Macromolecules, 29 (1996) 1579–1583.
[20] D. Rana, K. Bag, S.N. Bhattacharyya, B.M. Mandal, Miscibility of poly(styrene-co-butyl acrylate) with poly(ethyl methacrylate): existence of Both UCST and LCST, J. Polym. Sci., 38 (2000) 369–375.
[21] B. Schneier, Polymer compatibility, J. Appl. Polym. Sci., 17 (1973) 3175–3185.
[22] M.L. Masheane, A.R.D. Verliefde, S.D. Mhlanga, PES/quaternized-PES blend anion exchange membranes: investigation of polymer compatibility and properties of the blend, J. Membr. Sci. Res., 4 (2018) 93–100.
[23] M. Yang, T. Liu, The permeation performance of polyacrylonitrile/polyvinylidine fluoride blend membranes, J. Membr. Sci., 226 (2003) 119–130.
[24] S. Xu, Y. Liu, Y. Yu, X. Zhang, J. Zhang, Y. Li, PAN/PVDF chelating membrane for simultaneous removal of heavy metal and organic pollutants from mimic industrial wastewater, Sep. Purif. Technol., 235 (2020) 116185 (1–9), doi: 10.1016/j.seppur.2019.116185.
[25] M. Masuelli, J. Marchese, N.A. Ochoa, SPC/PVDF membranes for emulsified oily wastewater treatment, J. Membr. Sci., 326 (2009) 688–693.
[26] A. Subramania, N.T.K. Sundaram, G.V. Kumar, Structural and electrochemical properties of micro-porous polymer blend electrolytes based on PVdF-co-HFP-PAN for Li-ion battery applications, J. Power Sources, 153 (2006) 177–182.
[27] X. Zhu, H.-E. Loo, R. Bai, A novel membrane showing both hydrophilic and oleophobic surface properties and its non-fouling performances for potential water treatment applications, J. Membr. Sci., 436 (2013) 47–56.
[28] Y. Xiuli, C. Hongbin, W. Xiu, Y. Yongxin, Morphology and properties of hollow-fiber membrane made by PAN mixing with small amount of PVDF, J. Membr. Sci., 146 (1998) 179–184.
[29] N. Peng, T.S. Chung, K.Y. Wang, Macrovoid evolution and critical factors to form macrovoid-free hollow fiber membranes, J. Membr. Sci., 318 (2008) 363–372.
[30] S.X. Da, J. Wang, H.Z. Geng, S.L. Jia, C.X. Xu, L.G. Li, P.P. Shi, G. Li, High adhesion transparent conducting films using graphene oxide hybrid carbon nanotubes, Appl. Surf. Sci., 392 (2017) 1117–1125.
[31] W. Wang, L. Zhu, B. Shan, C. Xie, C. Liu, F. Cui, G. Li, Preparation and characterization of SLS-CNT/PES ultrafiltration membrane with antifouling and antibacterial properties, J. Membr. Sci., 548 (2018) 459–469.
[32] B. Arash, Q. Wang, V.K. Varadan, Mechanical properties of carbon nanotube/polymer composites, Sci. Rep., 4 (2014) 6479 (1–8), doi: 10.1038/srep06479.
[33] S. Majeed, D. Fierro, K. Buhr, J. Wind, B. Du, A. Boschetti-de-Fierro, V. Abetz, Multi-walled carbon nanotubes (MWCNTs) mixed polyacrylonitrile (PAN) ultrafiltration membranes, J. Membr. Sci., 403–404 (2012) 101–109.
[34] C. Liu, W. Wang, Y. Li, F. Cui, C. Xie, L. Zhu, B. Shan, PMWCNT/PVDF ultrafiltration membranes with enhanced antifouling properties intensified by electric field for efficient blood purification, J. Membr. Sci., 576 (2019) 48–58.
[35] V. Vatanpour, N. Haghighat, Improvement of polyvinyl chloride nanofiltration membranes by incorporation of multiwalled carbon nanotubes modified with triethylenetetramine to use in treatment of dye wastewater, J. Environ. Manage., 242 (2019) 90–97.
[36] Winarto, E. Yamamoto, K. Yasuoka, Separation of water–alcohol mixtures using carbon nanotubes under an electric field, Phys. Chem. Chem. Phys., 21 (2019) 15431–15438.
[37] Y. Huang, C. Xiao, Miscibility and mechanical properties of quaternized polysulfone/ benzoyl guar gum blends, Polymer, 48 (2007) 371–381.
[38] P. Wu, L.Y. Jiang, B. Hu, Fabrication of novel PVDF/P(VDF-co-HFP) blend hollow fiber membranes for DCMD, J. Membr. Sci., 566 (2018) 442–454.
[39] S. Panahian, A. Raisi, A. Aroujalian, Multilayer mixed matrix membranes containing modified-MWCNTs for dehydration of alcohol by pervaporation process, Desalination, 355 (2015) 45–55.
[40] J. Saadati, M. Pakizeh, Separation of oil/water emulsion using a new PSf/pebax/F-MWCNT nanocomposite membrane, J. Taiwan Inst. Chem. Eng., 71 (2017) 265–276.
[41] I.M. Wienk, R.M. Boom, M.A.M. Beerlage, A.M.W. Bulte, C.A. Smolders, H. Strathmann, Recent advances in the formation of phase inversion membranes made from amorphous or semi-crystalline polymers, J. Membr. Sci., 113 (1996) 361–371.
[42] J.-J. Li, Y.-N. Zhou, Z.-H. Luo, Polymeric materials with switchable superwettability for controllable oil/water separation: a comprehensive review, Prog. Polym. Sci., 87 (2018) 1–33.
[43] O. Marie, F.T. Starzyk, J.C. Lavalley, Confirmation of strongest nitrile-hydroxy groups interaction in the side pockets of mordenite zeolites, Phys. Chem. Chem. Phys., 2 (2000) 5341–5349.
[44] H. Zarrabi, M.E. Yekavalangi, V. Vatanpour, A. Shockravi, M. Safarpour, Improvement in desalination performance of thin film nanocomposite nanofiltration membrane using amine-functionalized multiwalled carbon nanotube, Desalination, 394 (2016) 83–90.
[45] X. Zhao, L. Cheng, R. Wang, N. Jia, L. Liu, C. Gao, Bioinspired synthesis of polyzwitterion/titania functionalized carbon nanotube membrane with superwetting property for efficient oil-in-water emulsion separation, J. Membr. Sci., 589 (2019), 117257 (1–9) doi: 10.1016/j.memsci.2019.117257.
[46] J. Saththasivam, W. Yiming, K. Wang, J. Jin, Z. Liu, A novel architecture for carbon nanotube membranes towards fast and efficient oil/water separation, Sci. Rep., 8 (2018) 7418 (1–6), doi: 10.1038/s41598-018-25788-9.
[47] J.N. Coleman, U. Khan, W.J. Blau, Y.K. Gun'ko, Small but strong: a review of the mechanical properties of carbon nanotube–polymer composites, Carbon, 44 (2006) 1624–1652.
[48] G.R. Guillen, Y. Pan, M. Li, E.M. Hoek, Preparation and characterization of membranes formed by nonsolvent induced phase separation: a review, Ind. Eng. Chem. Res., 50 (2011) 3798–3817.